## COMMUNICATION

Check for updates

# Interfacial halogen bonding with charge-transport layers for operational stability of hybrid perovskite solar cells

Jovan N. Lukić, [ID] †[ab] Weifan Luo,†[ac] Sunju Kim,†[d] Lydia Ferrer,†[e] Javier Ortiz, [ID][e] Desiré Molina, [ID][e] Jongmin Kim,[d] Jose Arturo Venegas,[a] Paul Zimmermann,[f] Thanh-Danh Nguyen,[d] Alexander Hinderhofer, [ID][f] Frank Schreiber, [ID][f] Ángela Sastre-Santos, [ID] *[e] Ji-Youn Seo, [ID] *[d] Vuk V. Radmilović [ID] *[b] and Jovana V. Milić [ID] *[a]

Hybrid metal halide perovskites have emerged as some of the leading semiconductors in photovoltaics. Despite their remarkable power conversion efficiencies, these materials remain unstable under device operating conditions. One of the main instabilities relates to the interface with the contact layers in photovoltaic devices, such as metal oxides. We rely on halogen bonding (XB) using 1,4-diiodotetrafluorobenzene (TFDIB) to modulate the interface of the TiO₂ electron-transport layer, demonstrating the improvement of perovskite solar cell operational stability. Furthermore, we complement this strategy with the use of iodo-functionalized Zn−phthalocyanine modulator of the hole-transporting material, which passivate the interface while enhancing the power conversion efficiency, showcasing the potential of XB in hybrid photovoltaics.

Halogen bonding (XB) has been recently applied to metal halide perovskites[1] as a strategy to increase operational stability, passivate trap sites, and suppress ion migration responsible for instabilities during device operation.[2,3] The basic principle of XB involves a highly polarised donor (D) based on an electrophilic halogen atom (X = I, Br, Cl), which can interact with the electron lone pair of a nucleophilic acceptor (A; Fig. 1), through the electropositive region referred to as the σ-hole.[2,3] The anisotropic distribution of the electron density in halogen-bonded atoms allows for high directionality,[2,3] whereas the strength of XB depends on the type of halogen atom, polarizability, and electron-attracting capability of the donor.[2,4] XB agents were found to affect hybrid perovskite structures through interaction with the surface,[2] passivating

defects such as terminal iodide groups in the perovskite framework, and improving crystallinity, stability, and power conversion efficiency.[3] Organic moieties used for XB are haloalkynes, haloalkenes, and haloarenes, whereas bifunctional systems[3,5] can also be applied to the interface of the perovskite and contact layer in a device. This could be beneficial since the interaction between the halide perovskite absorber and charge-transfer layer, such as metal oxides, can contribute to the improvement of charge-transfer properties and mechanical reliability.[6,7] To this end, XB could enable tuning electrical, chemical, and physical properties, as well as charge carrier
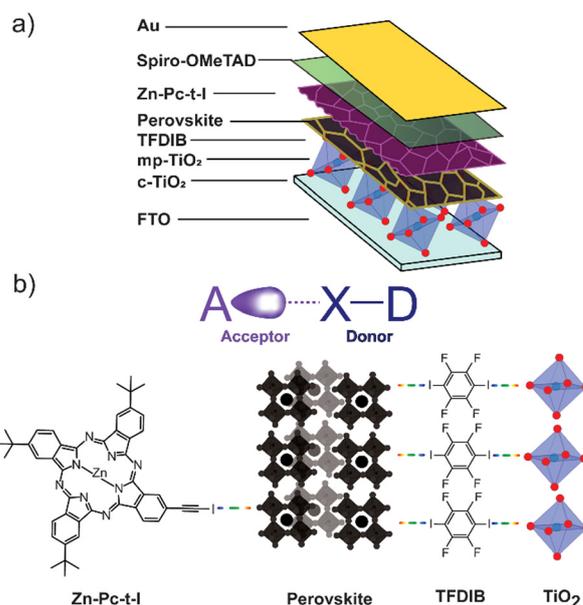


Fig. 1 Halogen bonding in hybrid halide perovskites. (a) Schematic of perovskite solar cells and (b) halogen bonding (XB) at the interface with the perovskite. FTO = fluorine-doped tin oxide; c = compact; mp = mesoporous; TFDIB = 1,4-tetrafluorodiiodobenzene; spiro-OMeTAD = 2,2′,7,7′-tetrakis[N,N-di(4-methoxyphenyl)amino]-9,9′-spirobifluorene; Zn-Pc-t-I = Zn-iodo-phthalocyanine.

[a] Adolphe Merkle Institute, University of Fribourg, Fribourg, Switzerland

[b] Faculty of Technology and Metallurgy, University of Belgrade, Belgrade, Serbia

[c] Chengdu University of Information Technology, School of Optoelectronic Engineering, China

[d] Department of Nanoenergy Engineering, Pusan National University, South Korea

[e] Institute of Bioengineering, University Miguel Hernández de Elche, Elche, Spain. E-mail: asastre@umh.es

[f] Institute of Applied Physics, University of Tübingen, Tübingen, Germany

† These authors contributed equally to this manuscript.

dynamics,[8] affecting overall optoelectronic characteristics and the stability of the devices.[9,10] An effective approach to increasing operational stability is through modulation at the interface of selective charge transport layers.[11–13] To this end, haloacetates were used for XB between $TiO_2$ and the perovskite layers; however, their XB interactions were not unambiguously assessed.[3,8] On the contrary, a bifunctional agent, 1,4-diiodotetrafluorobenzene (TFDIB), was found to interact with the hybrid perovskite surface through XB.[2,12] Despite the potential of TFDIB to enhance the operational stability of perovskite devices through the suppression of ion migration and the increase of hydrophobicity, it remains underexploited in this context.[6]

To improve charge injection and stability in perovskite solar cells, it is essential to address the interface with charge-selective transport layers, namely the hole transporting material (HTM) and the electron transfer layer (ETL). The most frequently used HTM, 2,2′,7,7′-tetrakis[N,N-di(4-methoxyphenyl)-amino]-9,9′-spirobifluorene (spiro-OMeTAD) has low hole mobility, which limits efficient charge extraction.[14] This requires doping that compromises stability, stimulating the use of alternative systems, such as those based on phthalocyanines[15,16] that exhibit increased stability.[17–20] Phthalocyanines (Pcs) are macrocyclic compounds that have been used in both n–i–p and p–i–n perovskite solar cell architectures. They have been employed in these systems as additives, passivating agents, and interlayers. As HTMs, Pcs have emerged as promising alternatives due to their enhanced stability, particularly when applied without dopants. Their molecular assemblies have been used to improve the stability and charge transfer to the active perovskite layers.[17,21] The use of XB in conjunction with such alternative HTMs could offer an unexplored opportunity to advance perovskite photovoltaics.

Here, we rely on XB at the interface with electron and hole-transport layers in perovskite solar cells by using TFDIB with $TiO_2$ and Zn-iodo-ethynyl-phthalocyanine (Zn-Pc-t-I) with spiro-OMeTAD charge-transport layers, respectively (Fig. 1). We investigate the effects using a combination of structural and optoelectronic techniques to assess the influence of XB on the performance and stability of perovskite photovoltaics in a model system applicable more broadly beyond this study.

We assessed the role of XB in conventional 3D triple cation hybrid perovskite materials of $Cs_{0.05}FA_{0.85}MA_{0.10}Pb(I_{0.97}Br_{0.03})_3$ composition[22] and the corresponding perovskite solar cell devices (Fig. 1(a) and 2) based on the fluorine doped tin oxide (FTO)/compact (c-) $TiO_2$/mesoporous (mp-) $TiO_2$/perovskite/spiro-OMeTAD/Au architecture following the procedure detailed in the Experimental section (SI). For this purpose, we treated the interface of the mp-$TiO_2$ layer with TFDIB at different concentrations (0.5 mg mL$^{-1}$, 1 mg mL$^{-1}$, and 2 mg mL$^{-1}$) and analysed the effect at the interface. The untreated films were referred to as reference, whereas TFDIB-treated films had TFDIB at the interface with $TiO_2$ to assess the effect of XB on the ETL. In addition, Zn-Pc-t-I (Fig. S1 and S2) was synthesised and characterised using nuclear magnetic resonance (NMR) spectroscopy (Fig. S3) and matrix-assisted laser desorption/ionization time-of-flight mass (MALDI-TOF)
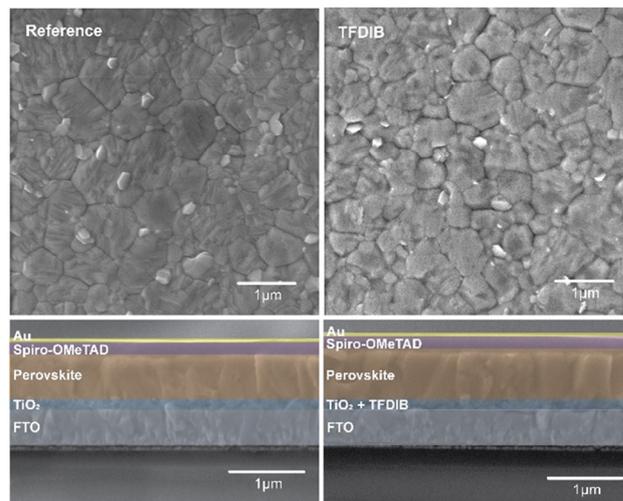


Fig. 2 Morphology of the perovskite thin films and devices. Top: SEM image of the morphology of the triple cation 3D perovskite reference (left) and TFDIB-treated (right) perovskite films. Bottom: cross-section SEM of the reference (left) and TFDIB-treated (right) solar cell device. The estimated thicknesses of the layers were: FTO ∼ 458 nm, $TiO_2$ ∼ 176 nm, perovskite ∼657 nm, spiro-OMeTAD ∼ 259 nm, Au ∼ 80 nm.

spectrometry (Fig. S4), as well as via Fourier transform infrared (FTIR) spectroscopy (Fig. S5), differential pulse voltammetry (DPV, Fig. S6), and steady-state UV-vis absorption and photoluminescence (PL) spectroscopy (Fig. S7). The Zn-Pc-t-I was thereafter applied as a molecular modulator at the interface with the HTM (spiro-OMeTAD), as well as simultaneously with TFIDB in representative solar cell devices to compare the effects of XB on different charge-transport layers.

The difference in morphologies of the perovskite thin films upon TFDIB and Zn-Pc-t-I treatment was not apparent from the scanning electron microscopy (SEM) images (Fig. 2 and Fig. S8, top). Both the reference and treated SEM images had bright $PbI_2$ crystallites, whereas the estimated average grain size of the Zn-Pc-t-I treated films was larger (Fig. S8), suggesting an existing interaction with the surface.[3] The SEM cross-section of the devices (Fig. 2, bottom) also suggested minor differences in morphologies with comparable thickness of the device layers.

The structural properties of the samples treated with TFDIB were further analysed by X-ray diffraction (XRD; Fig. 3(a)). The corresponding XRD patterns displayed additional peaks around 12.7°, which were likely from the excess $PbI_2$ used in the composition (Fig. 3(a)), with no significant difference in the structure of the perovskite phase upon treatment, irrespective of the concentration of TFDIB. This suggests that the structural integrity of the perovskite phase was preserved in the presence of TFDIB.[12] Complementary measurements, such as grazing incidence wide-angle X-ray scattering (GIWAXS; Fig. S9) corroborated this,[23] whereas the X-ray photoelectron spectroscopy (XPS) of the films on mp-$TiO_2$ showed no apparent change in the surface chemistry. This was evident through the absence of change in the core level peaks of O 1s, C 1s, and Pb 4f for both surface and deep profiles (Fig. S10 and S11), in accordance with the weak noncovalent interactions that are expected for
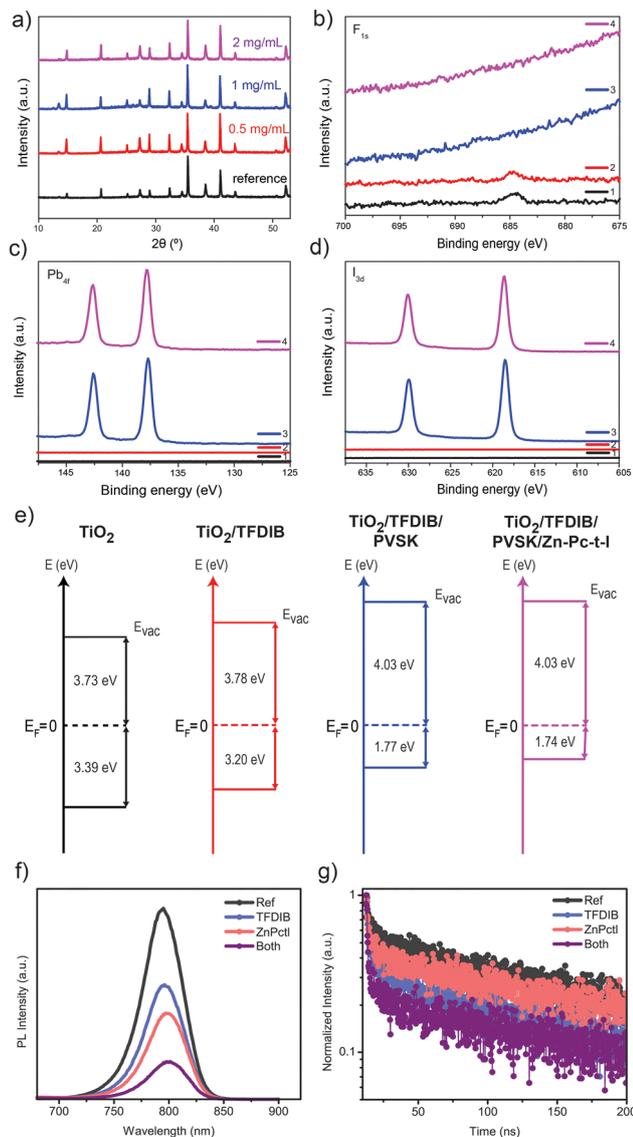
**Fig. 3** Structural and optoelectronic characteristics of XB perovskite films. (a) XRD patterns of perovskite films before (reference) and after treatment with three concentrations of TFDIB. Additional structural data shown in Fig. S9. Core level spectra (b) F 1s, (c) Pb 4f and (d) I 3d for condition 1 ($TiO_2$, black), condition 2 ($TiO_2$/TFDIB, red), condition 3 ($TiO_2$/TFDIB/perovskite, blue) and condition 4 ($TiO_2$/TFDIB/perovskite/Zn-Pc-t-I, purple) samples on glass; core level spectra of O 1s and C 1s shown in Fig. S10. (e) Energy level diagram for $TiO_2$, $TiO_2$/TFDIB, $TiO_2$/TFDIB/perovskite and $TiO_2$/TFDIB/perovskite/Zn-Pc-t-I films. (f) Steady-state and (g) time-resolved PL spectra of reference TFDIB and Zn-Pc-t-I XB-treated perovskite films (combined treatment indicated as "both" in the legend of the graphs).

XB. Moreover, the I 3d core level spectra featured a minor shift to lower energies upon TFDIB treatment, suggesting an XB interaction. The XPS data (Fig. 3(b)–(d)) did not indicate other changes in surface chemistry of perovskite thin films (Fig. S12). We have thereby assessed the differences in surface energetics upon treatment. For this purpose, the band alignment was acquired using ultraviolet photoemission spectroscopy (UPS, Fig. 3(e)). The work function (Fig. S13) for treated and reference samples had a difference of 0.02 eV, whereas the valence band

(VB) for the treated samples decreased by 0.06 eV. Based on the values for the VB and the work function acquired by Kelvin probe force (KPFM) microscopy for $TiO_2$ and $TiO_2$/TFDIB films (Fig. S14), TFDIB offered a suitable energy level alignment for charge extraction.[24] The corresponding changes in interfacial energetics are expected to affect optoelectronics.

The effect of TFDIB on optoelectronic properties was analysed by steady-state (Fig. 3(f)) and time-resolved photoluminescence (PL) spectroscopy (Fig. 3(g)). The PL spectra of the TFDIB-treated perovskite films revealed an energy bandgap of around 1.5 eV with an emission peak at around ~800 nm and an approximately 13 nm Stokes shift (Fig. S15), characteristic of mixed-cation mixed-halide perovskite compositions.[25] The intensity of the PL spectra decreased with the treatment of TFDIB, Zn-Pc-t-I, and the combination of both (Fig. 3(f)), indicating a difference in interfacial charge extraction. The impact on the charge carrier dynamics was further analysed by time-resolved photoluminescence (TRPL) spectroscopy (Fig. 3(g)). The films treated with TFDIB or Zn-Pc-t-I had shorter charge carrier lifetimes as compared to the reference, suggesting contributions to charge extraction. The films with both TFDIB and Zn-Pc-t-I featured an even shorter charge carrier lifetime, suggesting a combined effect on charge transport, which was expected to affect their use in photovoltaics.

The photovoltaic (PV) characteristics of the devices were assessed by monitoring the current–voltage (J–V) characteristics and estimating the PV metrics (Fig. 4(a) and (b)), namely power conversion efficiency (PCE), fill factor (FF), short circuit current ($J_{sc}$), and open circuit voltage ($V_{oc}$). The champion reference devices had PCE values up to 20.27% with FF of 0.755, $J_{sc}$ of 24.9 mA cm$^{-2}$, and $V_{oc}$ of 1.077 V, displaying a noticeable hysteresis loop between the reverse and forward bias (Fig. 4(a)). These PV characteristics were comparable to those of previously reported systems of the same halide perovskite composition.[22] The integrated short-circuit currents were also comparable to those estimated by incidence photon to current efficiency (IPCE) spectra (Fig. S16), excluding any significant spectral mismatch. On the contrary, the performances of TFDIB-treated devices were either similar to or lower than the reference, decreasing with the concentration of TFDIB. The champion devices featured PCE of 19.7% with an FF of 0.746, $J_{sc}$ of 25.35 mA cm$^{-2}$, and $V_{oc}$ of 1.043 V. The Zn-Pc-t-I-treated devices showed the highest PV parameters with a PCE value of 21.1%, an FF of 0.77, $J_{sc}$ of 25.72 mA cm$^{-2}$, and $V_{oc}$ of 1.063 V, indicating the effect of XB on photovoltaic metrics (Fig. 4(b)). In contrast, TFDIB and simultaneous treatments were not found to improve the photovoltaic performance of the devices, suggesting a level of incompatibility with the TFDIB-based treatment of the ETL, which can be associated with its orientation and hydrophobicity. In contrast, Zn-Pc-t-I-treated devices exhibited consistent improvements in PV performance, indicating a higher efficiency of XB at the interface with the HTM that is relevant beyond this study. Although the champion performance compares closely with similar compositions and film preparation conditions,[22] the overall performance can be further optimized. The XB was still envisaged to affect stability.
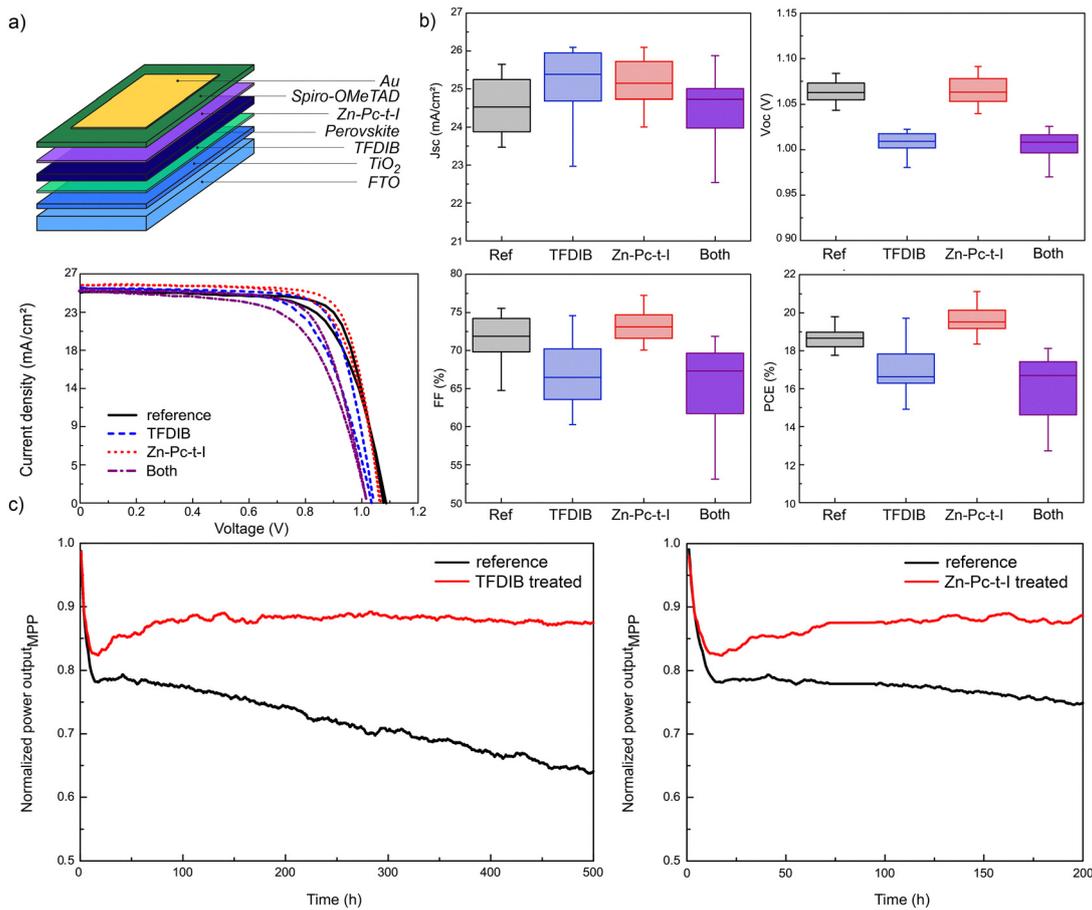
Fig. 4 Photovoltaic characteristics of perovskite solar cells. (a) Device architecture (top) and $J$–$V$ curves (bottom) under forward and reverse bias for champion reference (black), TFDIB (blue), and Zn-Pc-t-I-treated (red) perovskite solar cell devices, as well as those containing both XB agents (purple). (b) Photovoltaic metrics for PCE, $J_{sc}$, $V_{oc}$, and FF for reference (black) devices and those with TFDIB (blue), Zn-Pc-t-I (red), and simultaneous TFDIB and Zn-Pc-t-I treatment (indicated as "both" in purple). (c) Operational stability measurements for TFDIB-treated (0.5 mg mL$^{-1}$, red) samples without (left) and with (right) Zn-Pc-t-I (0.5 mg mL$^{-1}$ Zn-Pc-t-I) compared to reference devices (black) by maximum power point (MPP) tracking under illumination (1 sun) at ambient temperature in a N$_2$ atmosphere over time.

Operational stabilities were analysed by monitoring the photovoltaic performance at maximum power point (MPP) over time under continuous illumination (1 sun) and an inert (N$_2$) atmosphere at ambient temperature (Fig. 4(c)). The reference devices stabilised over time, which was indicated by the lower hysteresis shown by their hysteresis index (HI) (0.22 for reference; 0.25 for 0.5 mg mL$^{-1}$; 0.34 for 1 mg mL$^{-1}$ TFDIB) and after stabilisation (0.05 for reference, 0.19 for 0.5 mg mL$^{-1}$; 0.21 for 1 mg mL$^{-1}$ TFDIB) upon forward and reverse bias (Fig. S17). TFDIB-treated device hysteresis was not significantly affected, likely due to the effect of XB on interfacial ion migration.[2,3,26]

This was envisaged to affect operational stability and resulted in an increase in the stability for the TFDIB-treated device compared to the reference (Fig. 4(c)). This could also be seen for the higher concentration of TFDIB (1 mg mL$^{-1}$), although the layer could act as a barrier for charge extraction. However, the high-concentration-based and reference devices exhibited a typical "burn-in" effect, involving a sudden drop in performance within the first few hours, likely associated with ion migration upon light illumination and electrical

stress.[27–29] In contrast, the TFDIB-treated system at lower concentrations (0.5 mg mL$^{-1}$) displayed an initial rise in performance, followed by a decrease, suggesting possible charge accumulation.[30] The initial rise in efficiency during operation was also associated with the HTM-treated devices during the first 200 h. As a result, XB-treated devices at the interface of both charge-extraction layers showed enhanced stabilities. While the overall performance can be further optimised, this showcases the potential of the XB strategy in the interfacial stabilisation of perovskite solar cells.

## Conclusions

In summary, we analysed the effect of halogen bonding (XB) at the interface between perovskite and the charge-transfer layers in perovskite solar cells by using a TFDIB modulator at the TiO$_2$ and Zn-Pc-t-I at the spiro-OMeTAD interface in n–i–p perovskite solar cells. We investigated the effects at the interface, including morphological and structural changes, as well as

optoelectronic properties. The structural characteristics revealed no difference in the orientation of the perovskite films after treatment; however, films treated with a lower concentration (0.5 mg mL$^{-1}$) exhibited improved charge extraction. This was corroborated by the time-resolved PL spectroscopy and reflected in the photovoltaic characteristics and operational stability of perovskite solar cells. In addition, Zn-Pc-t-I-treated devices showed increased photovoltaic characteristics. However, devices simultaneously treated with Zn-Pc-t-I and TFDIB did not show photovoltaic improvements. The devices exhibited a reduced hysteresis upon treatment, indicating the effects on ion migration. While this resulted in inferior performances of the TFDIB-treated devices, it provided enhancements in operational stability. In contrast, the use of Zn–iodide–phthalocyanine at the interface with the hole-transport material improved both the operational stability and photovoltaic performance. Further optimisation can improve the overall device performance across conditions. This approach holds promise in advancing perovskite solar cells as well as other optoelectronic devices relying on interfacial XB.

## Author contributions

The manuscript was written by J. N. L. and W. L. through the support of all co-authors. The study was conceptualised by J. V. M., V. R., and Á. S.-S., while J. N. L. synthesised and fabricated perovskite thin films and devices with the support of W. L. and S.-J. K. under the supervision of J. V. M. and J.-Y. S. Moreover, L. F., J. O., and D. M. synthesized and characterized the Zn–phthalocyanine HTM under the supervision of Á. S.-S. Preliminary work for the phthalocyanine devices was done by J. A. V. under the supervision of J. V. M. GIWAXS measurements were performed by P. Z. under the supervision of A. H. and F. S., while T.-D. N. performed XPS, UPS, and KPFM measurements under the supervision of J.-Y. S. J. N. L. and V. V. R. acknowledge the Ministry of Science, Technological Development and Innovation of the Republic of Serbia (Contract No. 451-03-47/2025-01/200135 and PhD scholarship program) for support. Laser scribing system at Pusan National University was used in this work. All authors contributed to the manuscript.

## Conflicts of interest

There are no conflicts to declare.

## Data availability

Data can be accessed at the DOI: **https://doi.org/10.5281/zenodo.15658603**, and it is available under the license CC-BY-4.0 (Creative Commons Attribution-ShareAlike 4.0 International).

Supplementary information (SI): This involves the experimental section with materials and methods, as well as supplementary characterisation data. See DOI: **https://doi.org/10.1039/d5ya00166h**.

## Acknowledgements

## Notes and references

1 A. K. Jena, A. Kulkarni and T. Miyasaka, *Chem. Rev.*, 2019, **119**, 3036–3103.

2 M. L. Ball, J. V. Milić and Y.-L. Loo, *Chem. Mater.*, 2022, **34**, 2495–2502.

3 P. Metrangolo, L. Canil, A. Abate, G. Terraneo and G. Cavallo, *Angew. Chem., Int. Ed.*, 2022, **61**, e202114793.

4 M. Saccone and L. Catalano, *J. Phys. Chem. B*, 2019, **123**, 9281–9290.

5 L. Zhang, X. Liu, J. Li and S. McKechnie, *Sol. Energy Mater. Sol. Cells*, 2018, **175**, 1–19.

6 E. Ochoa-Martinez and J. V. Milić, *Nat. Energy*, 2021, **6**, 858–859.

7 Z. Dai, S. K. Yadavalli, M. Chen, A. Abbaspourtamijani, Y. Qi and N. P. Padture, *Science*, 2021, **372**, 618–622.

8 A. Mingorance, H. Xie, H. Kim, Z. Wang, M. Balsells, A. Morales-Melgares, N. Domingo, N. Kazuteru, W. Tress, J. Fraxedas, N. Vlachopoulos, A. Hagfeldt and M. Lira-Cantu, *Adv. Mater. Interfaces*, 2018, **5**, 1800367.

9 J. Wei, Q. Wang, J. Huo, F. Gao, Z. Gan, Q. Zhao and H. Li, *Adv. Energy Mater.*, 2021, **11**, 2002326.

10 F. Fiorentino, M. D. Albaqami, I. Poli and A. Petrozza, *ACS Appl. Mater. Interfaces*, 2022, **14**, 34180–34188.

11 L. Canil, J. Salunke, Q. Wang, M. Liu, H. Köbler, M. Flatken, L. Gregori, D. Meggiolaro, D. Ricciarelli, F. De Angelis, M. Stolterfoht, D. Neher, A. Priimagi, P. Vivo and A. Abate, *Adv. Energy Mater.*, 2021, **11**, 2101553.

12 M. A. Ruiz-Preciado, D. J. Kubicki, A. Hofstetter, L. McGovern, M. H. Futscher, A. Ummadisingu, R. Gershoni-Poranne, S. M. Zakeeruddin, B. Ehrler, L. Emsley, J. V. Milić and M. Grätzel, *J. Am. Chem. Soc.*, 2020, **142**, 1645–1654.

13 C. M. Wolff, L. Canil, C. Rehermann, N. Ngoc Linh, F. Zu, M. Ralaiarisoa, P. Caprioglio, L. Fiedler, M. Stolterfoht, S. Kogikoski, I. Bald, N. Koch, E. L. Unger, T. Dittrich, A. Abate and D. Neher, *ACS Nano*, 2020, **14**, 1445–1456.

14 N. A. N. Ouedraogo, G. O. Odunmbaku, B. Guo, S. Chen, X. Lin, T. Shumilova and K. Sun, *ACS Appl. Mater. Interfaces*, 2022, **14**, 34303–34327.

15 C. Rodríguez-Seco, L. Cabau, A. Vidal-Ferran and E. Palomares, *Acc. Chem. Res.*, 2018, **51**, 869–880.

16 D. Molina, J. Follana-Berná and Á. Sastre-Santos, *J. Mater. Chem. C*, 2023, **11**, 7885–7919.

17 P. Gao, K. T. Cho, A. Abate, G. Grancini, P. Y. Reddy, M. Srivasu, M. Adachi, A. Suzuki, K. Tsuchimoto, M. Grätzel and M. K. Nazeeruddin, *Phys. Chem. Chem. Phys.*, 2016, **18**, 27083–27089.

18 G. Reddy, K. Devulapally, N. Islavath and L. Giribabu, *Chem. Rec.*, 2019, **19**, 2157–2177.

19 D. Molina, M. A. Ruiz-Preciado, B. Carlsen, F. T. Eickemeyer, B. Yang, N. Flores-Díaz, M. J. Álvaro-Martins, K. Nonomura, A. Hagfeldt and Á. Sastre-Santos, *ChemPhotoChem*, 2020, **4**, 307–314.

20 P. Huang, A. Hernández, S. Kazim, J. Follana-Berná, J. Ortiz, L. Lezama, Á. Sastre-Santos and S. Ahmad, *ACS Appl. Energy Mater.*, 2021, **4**, 10124–10135.

21 M. Pegu, D. Molina, M. J. Álvaro-Martins, M. Castillo, L. Ferrer, P. Huang, S. Kazim, Á. Sastre-Santos and S. Ahmad, *J. Mater. Chem. C*, 2022, **10**, 11975–11982.

22 H. Zhu, Y. Liu, F. T. Eickemeyer, L. Pan, D. Ren, M. A. Ruiz-Preciado, B. Carlsen, B. Yang, X. Dong, Z. Wang, H. Liu, S. Wang, S. M. Zakeeruddin, A. Hagfeldt, M. I. Dar, X. Li and M. Grätzel, *Adv. Mater.*, 2020, **32**, 1907757.

23 L. Merten, A. Hinderhofer, T. Baumeler, N. Arora, J. Hagenlocher, S. M. Zakeeruddin, M. I. Dar, M. Grätzel and F. Schreiber, *Chem. Mater.*, 2021, **33**, 2769–2776.

24 B. Zhang, D. Gao, M. Li, X. Shang, Y. Li, C. Chen and T. Pauporté, *ACS Appl. Mater. Interfaces*, 2022, **14**, 40902–40912.

25 M. Baranowski, J. M. Urban, N. Zhang, A. Surrente, D. K. Maude, Z. Andaji-Garmaroudi, S. D. Stranks and P. Plochocka, *J. Phys. Chem. C*, 2018, **122**, 17473–17480.

26 X. Fu, M. Wang, Y. Jiang, X. Guo, X. Zhao, C. Sun, L. Zhang, K. Wei, H.-Y. Hsu and M. Yuan, *Nano Lett.*, 2023, **23**, 6465–6473.

27 R. Roesch, T. Faber, E. von Hauff, T. M. Brown, M. Lira-Cantu and H. Hoppe, *Adv. Energy Mater.*, 2015, **5**, 1501407.

28 M. V. Khenkin, E. A. Katz, A. Abate, G. Bardizza, J. J. Berry, C. Brabec, F. Brunetti, V. Bulović, Q. Burlingame, A. Di Carlo, R. Cheacharoen, Y.-B. Cheng, A. Colsmann, S. Cros, K. Domanski, M. Dusza, C. J. Fell, S. R. Forrest, Y. Galagan, D. Di Girolamo, M. Grätzel, A. Hagfeldt, E. Hauff, H. Hoppe, J. Kettle, H. Köbler, M. S. Leite, S. F. Liu, Y.-L. Loo, J. M. Luther, C.-Q. Ma, M. Madsen, M. Manceau, M. Matheron, M. McGehee, R. Meitzner, M. K. Nazeeruddin, A. F. Nogueira, Ç. Odabaşı, A. Osherov, N.-G. Park, M. O. Reese, F. De Rossi, M. Saliba, U. S. Schubert, H. J. Snaith, S. D. Stranks, W. Tress, P. A. Troshin, V. Turkovic, S. Veenstra, I. Visoly-Fisher, A. Walsh, T. Watson, H. Xie, R. Yıldırım, S. M. Zakeeruddin, K. Zhu and M. Lira-Cantu, *Nat. Energy*, 2020, **5**, 35–49.

29 Y.-R. Wang, A. Senocrate, M. Mladenović, A. Dučinskas, G. Y. Kim, U. Rothlisberger, J. V. Milić, D. Moia, M. Grätzel and J. Maier, *Adv. Energy Mater.*, 2022, **12**, 2200768.

30 N. T. P. Hartono, H. Köbler, P. Graniero, M. Khenkin, R. Schlatmann, C. Ulbrich and A. Abate, *Nat. Commun.*, 2023, **14**, 4869.